Tectonophysics 532–535 (2012) 167–174

Contents lists available at SciVerse ScienceDirect

Tectonophysics

journal homepage: www.elsevier.com/locate/tecto

A geometric frequency–magnitude scaling transition: Measuring $b = 1.5$ for large earthquakes

Mark R. Yoder [a,*], James R. Holliday [a], Donald L. Turcotte [b], John B. Rundle [a,b,c]

[a] Department of Physics, University of California Davis, Davis CA, USA
[b] Department of Geology, University of California Davis, Davis CA, USA
[c] Santa Fe Institute, Santa Fe NM, USA

ARTICLE INFO

Article history:
Received 26 August 2011
Received in revised form 20 December 2011
Accepted 27 January 2012
Available online 10 February 2012

Keywords:
Earthquake
Scaling large earthquakes
Earthquake rupture
Fractal dimension
Percolation
Frequency–magnitude scaling

ABSTRACT

We identify two distinct scaling regimes in the frequency–magnitude distribution of global earthquakes. Specifically, we measure the scaling exponent $b = 1.0$ for "small" earthquakes with $5.5 < m < 7.6$ and $b = 1.5$ for "large" earthquakes with $7.6 < m < 9.0$. This transition at $m_t = 7.6$, can be explained by geometric constraints on the rupture. In conjunction with supporting literature, this corroborates theories in favor of fully self-similar and magnitude independent earthquake physics. We also show that the scaling behavior and abrupt transition between the scaling regimes imply that earthquake ruptures have compact shapes and smooth rupture-fronts.

1. Introduction

It has long been recognized that earthquakes exhibit frequency–magnitude scaling so that (Gutenberg and Richter, 1954)

$$N(>m) = 10^{a-b\cdot m}. \quad (1)$$

$N(>m)$ indicates the number of earthquakes with magnitude greater than m; the parameter a measures the catalog's mean rate of seismicity, and the scaling exponent b measures the relative numbers of large to small earthquakes. Note that within the context of this paper, a "catalog" refers to any user-defined collection of earthquakes, nominally drawn from a standard source such as the Harvard Centroid Moment (CMT) or the Advanced National Seismic System (ANSS) databases.

Within a catalog, again for the scope of this paper, we draw little distinction between different magnitude measurement types — surface wave m_s, local m_l, or body wave m_b, except when necessary to be consistent with relevant literature. An exception to this rule is the moment magnitude m_w, which we sometimes specify to imply the accuracy of the magnitude measurement (Lay and Kanamori, 2011; Pacheco et al., 1992) or to indicate that the magnitude is related to scaling behaviors — a point that is discussed in some detail over the course of this paper. To first order, all magnitudes can be considered to be of unspecified measurement type m. In general, we use a number of different magnitudes, and other, symbols throughout this paper. The specific meaning of each symbol is defined in the text, and we have tried to use notation that is standard to the relevant literature. For example, consistent with canonical notation, the catalog completeness threshold m_c indicates the lower magnitude power law completeness limit of a catalog. Numbered magnitudes m_0, m_1, m_2, and so forth indicate some reference magnitude or sequence of magnitudes, as will be specifically defined in the accompanying text.

The value $b = 1$, in Eq. (1), is typically measured for small and moderate earthquakes, though locally observed values can range from approximately $0.8 < b < 1.2$ (Frohlich and Davis, 1993). Slip and rupture-length also scale with magnitude; these scaling relations have been shown to change for large earthquakes, $m > m_t$ where the "transition" magnitude m_t is approximately $7.5 \le m_t \le 7.6$ (Romanowicz and Ruff, 2002; Shaw, 2009; Shaw and Scholz, 2001). Similarly, Pacheco et al. (1992) observed a break in frequency–magnitude scaling, Eq. (1), for earthquakes of $m > m_t$, albeit with a limited catalog.

These observations have raised questions as to whether physical processes that are well understood for small earthquakes apply also to large magnitude events. This, in turn, has contributed to hypotheses of dynamic stress-drop and other deviations from self-similarity in earthquake related mechanics (Shaw, 2009). An alternative body of literature (Romanowicz and Ruff, 2002; Shaw, 2009; Shaw and Scholz, 2001) suggests that these large magnitude scaling behaviors result from geometrical constraints experienced by large ruptures

* Corresponding author. Tel.: +1 805 451 8750.
E-mail address: yoder@physics.ucdavis.edu (M.R. Yoder).

0040-1951/$ – see front matter © 2012 Elsevier B.V. All rights reserved.
doi:10.1016/j.tecto.2012.01.034

and can be explained, without introducing new physics, by building on the methodology proposed by Rundle (1989). In this paper, we find evidence supporting these latter theories, suggesting that the most fundamental physics of small earthquakes also applies to large earthquakes.

We revisit the analysis by Pacheco et al. (1992) with an improved catalog and show that global earthquakes exhibit at least two frequency–magnitude scaling domains with $b=1.009\pm0.00004$ for $5.5<m_w<m_t$ and $b=1.497\pm0.0015$ for $m_t<m_w<9.0$, noting that we have specified the moment magnitudes m_w. The magnitudes $m_w=5.5$ and $m_w=9.0$ are, respectively, the minimum magnitude completeness threshold and the largest magnitude in our catalog; the transition magnitude is $m_t=7.6$. We also show specifically that the domain $m_w>m_t$ introduces a distinct large-magnitude scaling regime, as opposed to upper magnitude truncation.

The significance of our result is threefold. First we confirm the transition at $m=m_t$, as suggested by Rundle (1989), and observed by Romanowicz and Ruff (2002), Shaw (2009), and Shaw and Scholz (2001) — each of which is discussed below, and our results corroborate the findings of Pacheco et al. (1992) with significantly improved statistical confidence. This suggests that, while earthquakes do appear to experience multiple scaling domains, the fundamental physics that govern earthquake rupture is self-similar over as many as 14 orders of magnitude (Kwiatek et al., 2010; Pacheco et al., 1992). Second, with respect to seismic risk assessment, these findings suggest that the frequency of $m>7.6$ earthquakes is significantly less than traditional GR scaling would predict. Finally, the abrupt transition between the two scaling regimes and observed b values indicate that earthquake rupture-fronts are smooth and that ruptures have compact shapes. We suggest that this can be described as a dynamic renormalization, similar to a framework presented by Saleur et al. (1996a,b).

2. Evidence of a geometric scaling transition

Lower magnitude saturation is observed in all catalogs that are not artificially truncated and is usually attributed to the limited sensitivity of the seismographic instrumentation network. Rundle (1993) used a statistical mechanics argument to show that, in addition to limited instrumentation, finite fault width can contribute to breakdown in scaling at small magnitudes. For a catalog from the Baldwin Hills section of the Newport–Ingelwood fault zone (Aki, 1987), Rundle (1993) obtains a lower limit characteristic magnitude $m_0=1.45$. This effect, however, is regionally sensitive; Kwiatek et al. (2010) find GR scaling down to $m=-4.4$ in deep gold mines in South Africa.

It is also possible to produce a catalog in which frequency–magnitude scaling appears to break down for the largest magnitudes. Physically, this suggests an upper limit to a local fault system's capacity to accumulate or release stress, typically associated with the length of the longest fault segment in the catalog. Large magnitude events, however, are rare, and it is difficult to exclude transient statistical fluctuations as an explanation for large magnitude truncation. Inaccurate magnitude assignment can also produce distributions that appear to be upper-truncated.

It has been suggested that some changes in scaling behaviors result from changes in stress-drop for very large (or very small) magnitude earthquakes, implying that the physics of large earthquakes differs from the physics of small earthquakes. The simplest theories, on the other hand, suggest that the underlying physics and most fundamental scaling relations are the same for large and small magnitude earthquakes. Most pointedly, these theories suggest that earthquake rupture processes, independent of magnitude, are characterized by area self-similarity or equivalently, constant stress-drop, a well known and accepted property of small earthquakes (Shaw, 2009). These theories suggest that the observed changes in scaling behaviors between large and small earthquakes, as discussed in the Introduction, are related to the geometry and number of degrees of freedom n_{dof} of the rupture; they do not require the introduction of new physics.

In general, the rupture area A can be expressed in terms of its spatial extent

$$A\propto L_s\cdot L_w, \tag{2}$$

where L_s and L_w are the orthogonal "surface" and "width" (or depth) components of the rupture in the plane of the fault surface, nominally parallel and perpendicular to the earth's surface respectively. L_s and L_w are often referred to as the "rupture length" and "rupture width." For small ruptures, $L_s\approx L_w\ll W$, where W is the depth of the brittle seismogenic zone of the lithosphere, or equivalently, the "width" of the fault. Assuming isotropy,

$$A\propto L_s^2. \tag{3}$$

For large ruptures where the surface rupture length $L_s>W$, $L_w\approx W$ is approximately constant, so

$$A\propto L_s\cdot W\propto L_s. \tag{4}$$

These large ruptures saturate the fault surface and scale in fractal dimension $D=1$, whereas a smaller rupture propagates across both dimensions ($D=2$) of the fault face.

With this geometry in mind, Rundle (1989) proposed an argument based on self-similarity, rupture dimension, and constant stress drop that predicts a frequency–magnitude scaling break with $b=1.0$ for small earthquakes, where $L_s<W$, and $b=1.5$ for large earthquakes, where $L_s\geq W$; the rupture length $L_s=W$ corresponds to $m_w\approx7.5$. Shaw and Scholz (2001), employing similar geometrical arguments, show that for large earthquakes, slip δ continues to increase with increasing rupture length, but at a much slower rate than for small earthquakes. This increase appears to asymptotically approach a maximum value and is considered to be associated with the variability in the thickness of the seismogenic lithosphere, which is consistent with the basic principle of fracture theory that slip δ is proportional to the smallest dimension of the rupture (Shaw, 2009). For a given location, the slip δ is constant for large, $L_s\geq W$, earthquakes. Consistent with this geometry, Romanowicz and Ruff (2002) observe a change in moment–rupture length scaling at approximately $M_0=3\cdot10^{27}$ dyne·cm, $m_w=7.6$. Specifically, they show that rupture length increases more rapidly, as a function of moment M_0, for large events than for small events. Based on similar geometrical arguments and assuming constant stress drop, Shaw (2009) shows three regimes of magnitude–rupture area scaling for $m>5$ earthquakes.

Pacheco et al. (1992) found that, for a global catalog, frequency–magnitude data fit a bi-linear model significantly better than a linear model. Their analysis, however, was subject to the catalogs of the time, which by their own suggestion were either inconsistent in magnitude assignment or too short to establish statistical confidence. We revisit their analysis with an improved catalog and also consider an upper magnitude truncated model. Of the three models linear, bi-linear, and upper-truncated, the bi-linear model produces the lowest reduced chi-square (χ_r^2) and Akaike Information Criteria (AIC) values, indicating the best fit to the data. In generalized notation,

$$\chi^2=\sum_i\left(\frac{y(x_i)-y_i}{\sigma_i}\right)^2, \tag{5}$$

$$\chi_r^2=\frac{1}{n_{dof}}\chi^2, \tag{6}$$

and

$$AIC = \chi^2 + 2 \cdot n_{\text{prams}}. \tag{7}$$

The ordered pairs (x_i, y_i) represent the data, with uncertainties σ_i, being fit to a model function $y(x)$. With respect to fitting data, $n_{dof} = N - n_{\text{prams}}$, where in this context N is the total number of data points and n_{prams} is the number of fitting parameters in $y(x)$.

For each of the three distributions, the set of fitting parameters that produces the minimum χ_r^2 also produces the minimum AIC value. Consistent with Pacheco et al. (1992) and Rundle (1989), we measure $b = 1.009 \pm 0.00004$ for $5.5 < m < m_t$ and $b = 1.497 \pm 0.0015$ for $m_t < m < 9.0$, where $m_t = 7.6 \pm 0.002$. These results are tabulated in Tables 1 and 2; the details of the fits are discussed in the next section.

3. Fitting the data

Our catalog includes all global events, available at the time of writing, from the Harvard CMT database. It consists of 35,465 events that occurred between the dates of January 1976 and September 2010, at depths up to 690 km, and is complete to a minimum magnitude of approximately $m_c = 5.5$. Of these 35,465 total earthquakes, there are 13,841 events with $m_w \geq m_c$ and 133 "large" events of $m_w \geq 7.5$. The same catalog at the end of 1991, as per Pacheco et al. (1992), consists of only 9862 events in total, 5530 of which were $m_w \geq 5.5$ and 43 of which were $m \geq 7.5$. Above the catalog completeness threshold, for all events $m > m_c$, the number of events N is known very precisely; the uncertainty in the catalog, with respect to frequency–magnitude statistics, is defined by the error in the moment tensor components $M_{ij} \pm \varepsilon_{ij}$.

The scalar moment M_0 is calculated by diagonalizing the moment tensor M_{ij}. Ideally, we expect of the eigenvalues M_j, $M_1 = -M_2$; $M_3 = 0$. The data are approximately consistent with this expectation, so the scalar moment M_0 is calculated by discarding the third eigenvalue and averaging the larger two,

$$M_0 = \frac{|M_1| + |M_2|}{2}. \tag{8}$$

Noting that the error components ε_{ij} themselves constitute a tensor, we calculate the uncertainty ε_j for each eigenvalue M_j by diagonalizing ε_{ij}. We treat M_j as independent and identically distributed (IID) random variables and estimate the scalar uncertainty ε_0 as

$$\varepsilon_0^2 = \varepsilon_1^2 + \varepsilon_2^2. \tag{9}$$

The moment magnitude m_w is

$$m_w \pm \varepsilon_m = \frac{2}{3}\log_{10}(M_0 \pm \varepsilon_0) - 10.7, \tag{10}$$

and we calculate the moment magnitude error ε_m from a Taylor expansion about M_0.

We employ six fitting methods, "Methods 1–6", and test three model distributions: linear (power law), bi-linear (broken power law), and an upper-magnitude truncated power law. These distributions, respectively, imply a single scaling domain, two distinct scaling domains, and scaling terminated by a maximum allowable magnitude. To facilitate direct comparison to Pacheco et al. (1992) and to ensure that we properly sample the parameter space, we present four fitting methods, Methods 1–4, to the bi-linear model and show that they yield similar results. In each case, we use a weighted least-squares method (Bevington and Robinson, 1992) and employ a standard converging algorithm (Jones et al., 2009). To facilitate a properly weighted least-squares fit, we fit the data in the dual space where N is treated as the independent variable and $m = m(N)$. For example, the dual form of Eq. (1) is

$$m(N) = \frac{a - \log[N]}{b}, \tag{11}$$

and we minimize the residual χ^2,

$$\chi^2 = \sum_i \left(\frac{m(N_i) - m_i}{\varepsilon_{mi}} \right)^2, \tag{12}$$

where N_i are the numbers of earthquakes with magnitudes $m > m_i$, from the data, and ε_{mi} is the uncertainty of the ith magnitude, as calculated from Eq. (10). Following Sornette et al. (1996), we refer to the dual $m(N)$ space as the "rank ordered" (RO) representation and the more conventional $N(m)$ space as the Gutenberg–Richter (GR) representation. We conduct the bulk of our discussion with respect to the GR representation — for example, the fitting parameters a and b are expressed with respect to Eq. (1).

For the bi-linear fits, we assume that the distribution breaks at some magnitude m_t. For Methods 1 and 2, we fit the data in the domains $m_c < m < m_t$ and $m > m_t$ separately; because the fitting algorithm does not simply converge on the m_t parameter, we sample the values $6.0 < m_t < 8.0$ in sequential steps of $\Delta m_t = 0.0001$. We select our fit parameters by two separate criteria. First (Method 1), following the treatment of Pacheco et al. (1992), we identify the break as the value of m_t that maximizes the difference of the slopes, $\Delta b = |b_1 - b_2|$, for the two domains. The uncertainties are determined by a standard least squares method (Bevington and Robinson, 1992) for each

Table 1
Least squares fit parameters for the weighted χ_r^2 method. Method 1: the domains $m_w < m_t$ and $m_w > m_t$ are fit separately; the best fit is determined by the set of parameters that maximize the slope difference between the two domains, $\Delta b = |b_1 - b_2|$. Method 2: the same as Method 1, except the parameters that minimize χ_r^2 over the full domain are chosen as the best fit. Method 3: the data are fit directly to Eq. (13); the minimum χ_r^2 parameters constitute the best fit. Method 4: same as Method 3, except the parameter space is sampled by a Monte Carlo method. Methods 5a and 6 are the minimum χ_r^2 (Jones et al., 2009) fit parameters to an upper-magnitude truncated power law and power law (linear), Eqs. (20) and (1) distributions, respectively.

Method	a_1	b_1	m_t	a_2	b_2	χ_r^2	AIC
1. Pacheco	8.16893	1.00913	7.6068	11.86393	1.49903	0.54050	7461.11
	±0.00031	±0.00015	±.0001	±0.00183	±0.00172		
2. bi-linear(a)	8.16817	1.00900	7.5441	11.84403	1.49655	0.53536	7390.08
	±0.00032	±0.00016	±.0001	±0.00174	±0.00163		
3. Bi-linear(b)	8.16816	1.00900	7.6036	11.84403	1.49655	0.53537	7397.74
	±0.00010	±0.00004	±.0001	±0.00161	±0.00150		
4. Bi-linear MC	8.15530	1.00645	7.7213	11.77254	1.49348	0.96235	13283.29
	±0.00007	±0.00004	±.00197	±0.00064	±0.00186		
5a. Eq. (20)	8.10870	0.99883	8.4843			0.95332	13162.63
6. Linear	8.26888	1.02502				6.48680	89554.29
	±0.00029	±0.00014					

Table 2
Least squares fit parameters for the unweighted χ_r^2 method. Otherwise, the fitting methods are identical to Table 1, with the exception that Method 5b uses an exponentially truncated power law, Eq. (19). The relative χ_r^2 and *AIC* values indicate that the bi-linear model (Methods 1–4) is a much better fit than the tapered power law, Eq. (19).

Method	a_1	b_1	m_t	a_2	b_2	χ_r^2	AIC
1. Pacheco	8.08361	0.99546	7.54000	11.68012	1.47584	0.000051	8.70
	±0.00085	±0.00014	±0.0001	±0.08290	±0.01058		
2. Bi-linear(a)	8.08053	0.99494	7.47000	11.59103	1.46478	0.000050	8.69
	±0.00085	±0.00014	±0.0001	±0.06776	±0.00871		
3. Bi-linear(b)	8.08047	0.99493	7.47000	11.59103	1.46478	0.000050	4.69
	±0.00085	±0.00014	±0.0001	±0.06799	±0.00874		
4. Bi-linear MC	8.09337	0.99710	7.49677	11.58046	1.46073	0.000055	8.75
	±0.00085	±0.00014	±0.08880	±0.08807	±0.01129		
5b. Eq. (19)	8.08276	0.99510	8.56727			0.00015	5.07
6. Linear	8.18188	1.01224				0.00039	9.40
	±0.00235	±0.00039					

domain separately. For our second set of fit parameters (Method 2), we use the same fitting technique above but select the set of parameters that minimizes the total reduced chi-square, χ_r^2, over the full domain.

For Methods 3 and 4, we fit the logarithms of the data directly to a bi-linear model

$$\log[N(m)] = \Theta(m_t - m)\cdot(a_1 - b_1\cdot m) + \Theta(m - m_t)\cdot(a_2 - b_2\cdot m), \tag{13}$$

where Θ is a heavy side step function such that $\Theta(x\geq 0)=1$ and $\Theta(x<0)=0$; a_1, b_1, a_2,and b_2 are the linear intercept and slope fit parameters for the data $m<m_t$ and $m>m_t$ respectively. The cumulative residual χ^2 in the RO space, for the purpose of fitting the model to the data, is

$$\chi^2 = \sum_i \frac{\left[m_i - \left(\Theta[N(m_i)-N(m_t)]\cdot\frac{a_1-\log[N_i]}{b_1} + \Theta[N(m_t)-N(m_i)]\cdot\frac{a_2-\log[N_i]}{b_2}\right)\right]^2}{\varepsilon_{mi}^2}. \tag{14}$$

We minimize χ^2 first (Method 3) using a converging least-squares algorithm (Jones et al., 2009); it was again necessary to sample the parameter m_t, which we did sequentially in $\Delta m_t = 0.0001$ steps. As a qualitative check (Method 4), we use a "brute force" fitting method in which we sample the parameter space by a Monte-Carlo method.

For each method, we measure approximately $b_1 = 1.0$, $b_2 = 1.5$, and $m_t = 7.6$, as anticipated theoretically by Rundle (1989), previously measured by Pacheco et al. (1992), and consistent with the methods employed by, Romanowicz and Ruff (2002), Shaw (2009), and Shaw and Scholz (2001). The precise values and their uncertainties are tabulated in Table 1. Note also that m_t specifically defines the divide between the large and small magnitude domains of the distribution. Because m_t is treated as a free parameter,

$$m_t \neq m_t' \equiv \frac{(a_2 - a_1)}{(b_2 - b_1)}, \tag{15}$$

where m_t indicates the position of the actual bend or break (the intersection of the lines) in the distribution; m_t can be readily calculated from Tables 1 and 2.

For our linear model (Method 6), we fit the data over the full domain $m>m_c$ according to Eqs. (11) and (12). The results are shown in Fig. 1 and Table 1. We address the question of an upper bound to earthquake magnitudes, or more generally large magnitude scaling degradation, by fitting the data to two upper truncated power law distributions (Method 5) — the tapered, or exponentially truncated, power law,

$$y(x) = y_0\cdot x^{-b} e^{-x/x_0}. \tag{16}$$

and the more abruptly terminating upper truncated power law (Burroughs and Tebbens, 2002),

$$y(x) = y_0\cdot\left(x^{-b} - x_0^{-b}\right). \tag{17}$$

In both cases, y_0 is a parameter, b is the scaling exponent, and x_0 parameterizes a characteristic upper-limit to the domain x.

With respect to earthquake magnitude statistics, we introduce the magnitude–moment substitution

$$M \equiv 10^m. \tag{18}$$

Substituting Eqs. (1) and (18) into Eqs. (17) and (16), with $x=M$, $y(x)=N(M)$, and $x_0=M_{\max}$, our tapered GR distribution is

$$N(>M) = 10^a\cdot M^{-b} e^{-M/M_{\max}}, \tag{19}$$

and our upper-truncated GR distribution is

$$N(>M) = 10^a\cdot\left(M^{-b} - M_{\max}^{-b}\right). \tag{20}$$

In both cases, we clearly recover Eq. (1) in the limit $M/M_{\max}\to 0$.

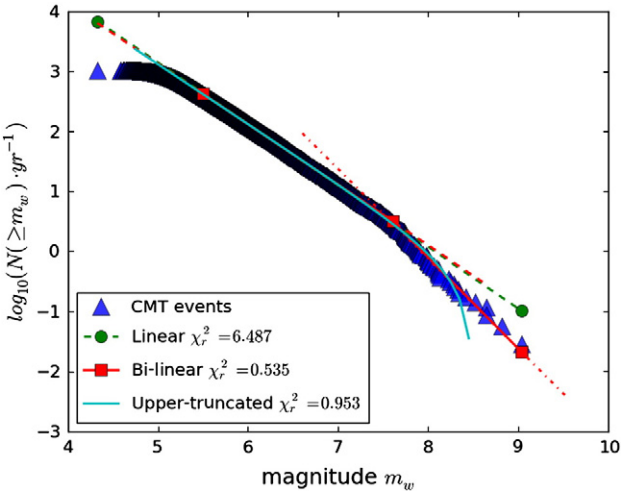

Fig. 1. The frequency–magnitude distribution of global earthquakes from the Harvard CMT catalog. The minimum completeness magnitude of the catalog is approximately $m_c = 5.5$. Data are shown in blue triangles; the bi-linear (broken power law) fit shown (red lines and square terminators) is from Method 3, as described in the text. We observe a break in scaling at approximately $m_t = 7.6$. The scaling exponents $b_1 = 1.009$, $b_2 = 1.497$. Also shown are the linear fit (green dashed line and circle terminators) and the upper-magnitude truncated, Eq. (20), fit (cyan solid line), Eq. (19).

We perform a weighted least-squares fit to Eq. (20), the dual form of which is

$$M(N) = 10^{a/b}\left(N + 10^{a} M_{\max}^{-b}\right)^{-1/b}, \tag{21}$$

and we tabulate the results in Table 1. Inverting Eq. (19), however, does not yield a closed-form solution, so a direct weighted least-squares fit is not possible (Holliday and Yoder, 2012). In light of this, we fit the data to Eq. (19) in the GR representation using an un-weighted least-squares method. For reference, we also repeat the linear and bi-linear fits, from above, using the un-weighted method; the results for these fits are listed in Table 2.

In both the weighted and un-weighted fits, we favor the bi-linear model over the linear and upper-truncated distributions on the basis of their respective minimum χ_r^2 and *AIC* values. While a direct weighted comparison of the exponentially truncated distribution, Eq. (19), to the bi-linear distribution, Eq. (13) would be desirable, we feel our combined analysis is sufficient to rule out upper magnitude truncation in favor of multiple scaling domains.

4. The shape and fractal dimension of earthquake rupture

In this section, we show that the shape and fractal dimension D of earthquake ruptures can be inferred from frequency–magnitude scaling. The shape and fractal dimension of a rupture is related to "fingering" phenomena observed in wildfire propagation, in which jets of flame shoot out in front of an advancing flame-front, effectively increasing its fractal dimension, or equivalently its surface area, and increasing its rate of propagation (Clark et al., 1996). Yoder et al. (2011) show that the rate of growth, intensity, and expected size of wildfires can be understood with respect to the shape and fractal dimension of fuel clusters. These principles can be extended to endemic processes in general; the earthquake analog of a wildfire propagating through a fuel cluster is a rupture propagating through a stress field. In both cases, low fractal dimension shapes ($D \to 1$) produce steeper frequency–magnitude scaling (fewer large events) than higher ($D \to 2$) dimension shapes.

We first introduce a generalized form of the standard calculation of earthquake rupture dimension (Aki, 1981). From Eq. (10), the seismic scalar moment M_0 is

$$M_0 = \mu A \delta, \tag{22}$$

where the parameter μ is the shear modulus, A is the area of the rupture, and δ is the slip. Noting from Eq. (3) that $A \approx L_s^2$, for small earthquakes, we suggest the generalized form,

$$M_0 \sim L_s^{\beta}, \tag{23}$$

where the exponent β is a parameter related to the number of degrees of freedom n_{dof} available to the rupture. Inserting Eqs. (10) and (23) into Eq. (1),

$$\log(N) = a - b\left(\frac{2}{3}\beta \log L_s - 10.7\right), \tag{24}$$

and so,

$$N \sim L^{-\frac{2}{3}\beta b} \sim L^{-D} \tag{25}$$

where $D = \frac{2}{3}\beta b$ is the fractal dimension (Aki, 1981). From Kanamori and Anderson (1975), we have

$$\delta_1 \propto L_s \tag{26}$$

for small $m < m_t$ earthquakes, and for large earthquakes, the slip is constant for a given fault width W (Shaw, 2009),

$$\delta_2 = \delta_0(W). \tag{27}$$

Given Eqs. (26) and (27), and substituting Eqs.(3) and (4) into Eq. (22), we infer from Eq. (23) that for small earthquakes, $\beta_1 = 3$ and for large earthquakes, $\beta_2 = 1$. The fractal dimensions of small and large earthquakes, respectively then, is $D_1 = 2b$ and $D_2 = 2b/3$. Given our measured values $b_1 = 1.009$ and $b_2 = 1.497$, $D_1 \approx 2$ and $D_2 \approx 1$. The integer values of D and the abrupt transition to the the $D = 1$ process, as seen in Fig. 1, indicate that earthquake ruptures are compact, not ramified, shapes. That is to say, rupture fronts are smooth and few, if any, unruptured "islands" are left behind in the rupture area.

The fractal dimension D of the rupture can alternatively be calculated with respect to the aspect ratio α of the rupture. This method illustrates a rupture dynamic that is potentially important to numeric earthquake simulators. Again, the measured scaling exponents $b_1 = 1.009$, $b_2 = 1.497$ indicate that the fractal dimension D of earthquake ruptures is very close to $D_1 = 2$ and $D_2 = 1$.

We start by writing the surface component of the rupture length L_s as a factor of its width L_w,

$$L_s = \alpha L_w, \tag{28}$$

where $\alpha \geq 1$ is a parameter, so Eq. (4) becomes

$$A = \alpha L_w^2. \tag{29}$$

We also suggest that the rupture area A scales with L_s

$$A = (\alpha L_w)^D, \tag{30}$$

where we have substituted Eq. (28) for the length L_s, and we acknowledge that Eq. (30), by itself, implies scaling only over domains where D is constant. The scaling exponent D, consistent with earlier notation, represents the fractal dimension of the rupture in the simple sense that for linear shapes, $D = 1$; for a square, circle, or other filled planar shape, $D = 2$, and for ramified clusters in a dimension $d = 2$ embedding space, $1 < D < 2$ (Stauffer and Aharony, 1994; Yoder et al., 2011).

To correct the units in Eq. (30) and to facilitate solving for D, we rewrite Eqs. (29) and (30) in terms of a unit length L_0, where

$$L_0 = \frac{L_w}{n_w}. \tag{31}$$

The parameter n_w, nominally an integer, defines the discretization of the length L_w. This introduces a discrete lattice representation of the rupture area $A = n_c L_0^2$, where n_c is the number of elements in the rupture cluster, and L_0 represents a minimum size, or discrete limit, for scaling behavior. In this discretely scale invariant representation, the size of the lattice elements is fixed; only the number of elements in the rupture cluster n_c scales,

$$n_c = (\alpha n_w)^D. \tag{32}$$

Setting Eqs. (29) and (30) equal to one another and substituting Eq. (32),

$$L_0^2 \alpha n_w^2 = L_0^2 (\alpha n_w)^D. \tag{33}$$

Solving for the fractal dimension D, we find

$$D = 1 + \frac{\log(n_w)}{\log(\alpha n_w)}, \tag{34}$$

the form of which might be recognized from Saleur et al. (1996b).

Eq. (34) has a number of implications. While an earthquake rupture length is less than the fault width, $L_s < W$, assuming self-similarity and a compact shape, $L_s \approx L_w$ ($\alpha = 1$), and so $D = 2$. Further, so long as $\alpha = 1$, $D = 2$ is infinitely degenerate for all values of n_w, with the exception of $\alpha n_w = 1$ exactly which is singular. When the rupture reaches the upper and lower fault boundaries, when $L_s > W$ ($\alpha > 1$), this symmetry with respect to n_w is broken. Clearly, as per Eq. (34) $D < 2$ for $\alpha > 1$, but significant and abrupt deviation from $D = 2$ requires that $\alpha \gg n_w$ or $n_w \approx 1$. In fact, $D = 1$ can only be achieved for $\alpha \to \infty$ or $n_w \to 1$, as shown in Figs. 2, 3, and 4.

Noting that the finite size of the earth and thickness of the lithosphere in seismogenic zones implies finite values for α, falling well within the range $1 < \alpha < 100$ (Turcotte and Schubert, 2002), we expect physically motivated solutions to reflect $n_w \to 1$ from above for large earthquakes. We also observe that power-law behavior, where D is constant, requires either $\alpha = 1$ or alternatively $n_w \to 1$ when $\alpha > 1$. This implies that a sharp transition between scaling regimes also requires $n_w \to 1$ in the domain $\alpha > 1$ ($m > m_t$). These expectations are consistent with Fig. 1, in which we observe two power-law regimes separated by a sharp transition at $m_w = m_t$. For small earthquakes ($m < m_t$), $b = 1.009$; $\alpha \to 1$ from above and $D \to 2$ from below. For large earthquakes ($\alpha > 1$), $b = 1.497$; $n_w \to 1$ from above, and $D \to 1.0$ from above. We show the transition from $D = 2$ to $D = 1$ as a function of n_w and α in Figs. 2 and 3, respectively, and we show simulated GR distributions for various n_w in Fig. 4.

The parameter L_0, then, indicates a physically significant characteristic size. For very simple n_x by n_y cellular automata (CA) models, including forest-fire (Drossel and Schwabl, 1992) and slider block (Carlson and Langer, 1989) models, L_0 defines the size of the lattice elements. We find that these models show little deviation from square models, even for extreme aspect ratios ($n_x \gg n_y$), until approximately $n_y < 10$. Given the proper rupture dynamics, or propagation dynamics in general, a line or curvelet of n_f grid elements may form a coherent rupture front so that as a rupture grows, $L_0 \propto n_f$. This can be thought of as a dynamic renormalization of the lattice from L_0 to $n_f \cdot L_0$. The sharp transition from $b = 1.009$ to $b = 1.497$ observed in Fig. 1 indicates that earthquake rupture exhibits this type of behavior; Figs. 2–4 corroborate this suggestion. Specifically, for large ruptures

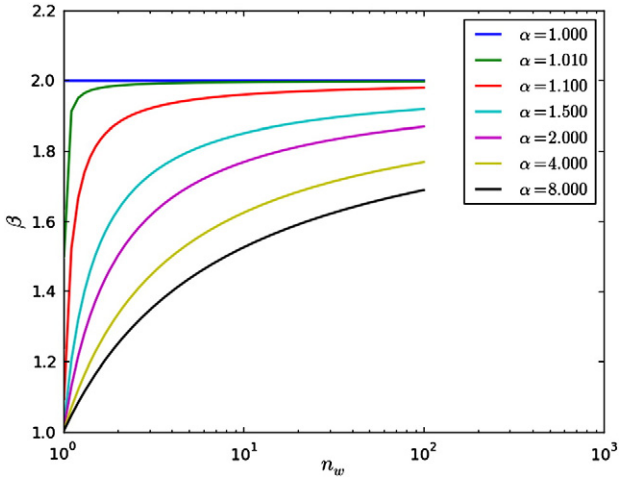

Fig. 2. Fractal dimension D, Eq. (34), as a function of n_w for $\alpha = 1.0$, 1.01, 1.1, 1.5, 2.0, 4.0, 8.0, from top to bottom. The fractal dimension D depends on both α and n_w. $D = 1$ occurs only for $n_w = 1$, except in the non-physical limit of $\alpha \to \infty$.

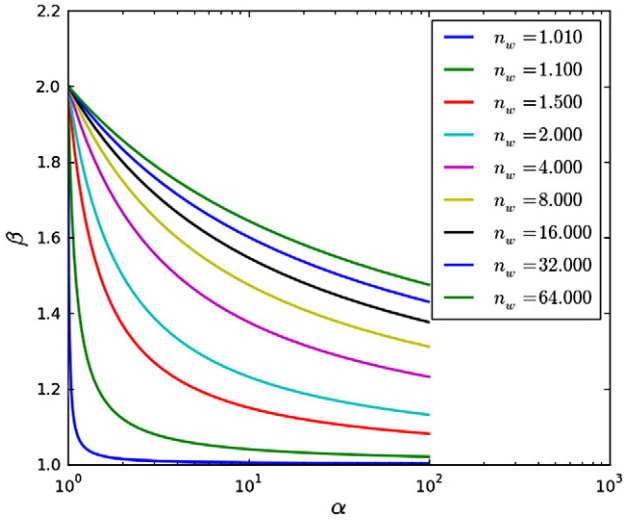

Fig. 3. The fractal dimension D, Eq. (34) as a function of α for $n_w = 1.01$, 1.1, 1.5, 2, 4, 8, 16, 32, 64, from bottom to top. Note the transition from $D = 2$ to $D \to 1$ occurs rapidly for $n_w \to 1$ but occurs more slowly with increasing α. Again, only for $n_w = 1$ do we get $D = 1$. Also note that we only get power-law behavior in Eq. (34) for $n_w = 1$.

$n_f \approx n_y$ so that $L_0 \approx W$ and effectively $n_w \approx 1$, equivalent to a renormalization to a lattice where $n_y = 1$.

Saleur et al. (1996a,b) present a theory for the renormalization group with respect to earthquakes that is related to this observation. This is also similar to the tiling argument made by Rundle (1989), in which the fault surface, orcellular automata lattice, is renormalized to elements of size $L_0 = L_w$, so that again effectively $n_w \approx 1$. With respect to real earthquakes, L_0 may be related to the speed at which a fracture propagates, or equivalently its range of interaction, and the shape or fractal dimension of the rupture front. Yoder et al. (2011) show a similar behavior in wildfires — specifically that a wildfire's intensity is related to its size, shape, and fractal dimension; its expected intensity, in turn, determines its persistence and ultimately the steepness (scaling exponent) of the frequency–magnitude distribution.

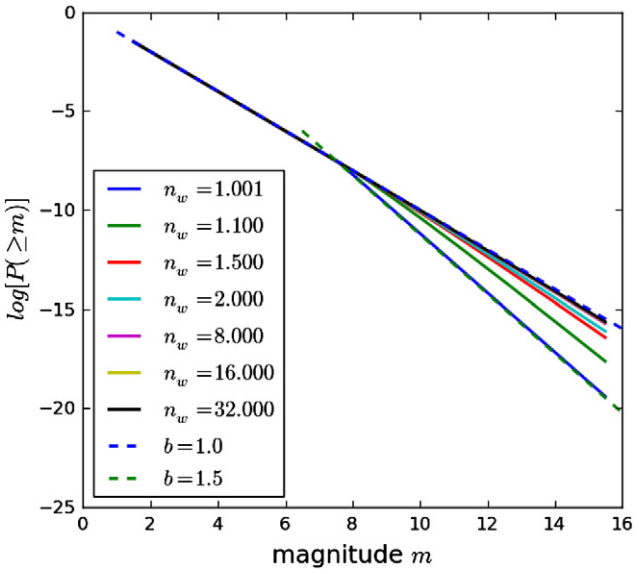

Fig. 4. Simulated GR distribution with a scaling break at $m = 7.5$. For $n_w \gg 1$, the distribution rolls gradually from $b = 1.0$ to $b = 1.5$; for $n_w \to 1$, the change is abrupt. These distributions are determined by assuming Eq. (1). The form for the scaling exponent $b = 3/(D+1)$, where D is the fractal dimension Eq. (34), can be inferred from Rundle (1989). Note that $b_{D=1} = 3/2$, $b_{D=2} = 1$, and $b(1 < D < 2)$ behave as expected from the discussion in Section 4.

5. Discussion

We fit the frequency–magnitude statistics of global earthquakes to three distributions — power law, broken power law, and two upper-truncated models. We favor the broken power law distribution on the basis of minimum χ_r^2 and *AIC* tests. We conclude that earthquakes experience at least two frequency–magnitude scaling domains with $b_1 = 1.009 \pm 0.00004$ for $5.5 < m_w < 7.6$ and $b_2 = 1.497 \pm 0.0015$ for $7.6 < m_w < 9.0$. The weighted bi-linear fits, Methods 1–4, yield nearly identical results, which is as expected since the main difference between them is the method by which they sample the parameter space. The unweighted fits also produce similar results; the consistency over multiple fitting methods attests to the legitimacy of the results. All of these methods yield results similar to parameters published by Pacheco et al. (1992) and anticipated by Rundle (1989). We further discuss the implications of this scaling transition with respect seismic hazard assessment and rupture dynamics.

In conjunction with supporting literature (Romanowicz and Ruff, 2002; Shaw, 2009; Shaw and Scholz, 2001), our findings suggest that the underlying physics of earthquake rupture is magnitude independent. The transition at $m_w = m_t$ can be understood with respect to the geometry of the rupture process, without introducing dynamic stress-drop or other non-self-similar physics for large magnitude events. Specifically, for small earthquakes, rupture is a $D = 2$ process along the fault surface; for large earthquakes, where the rupture length is greater than the depth of the seismogenic zone, $L_s > W$ as per Eqs. (2), (3), and (4), the process is approximately $D = 1$ along the fault surface.

Extending this reasoning to very small earthquakes suggests a class of events where the rupture length $L_s \approx L_\tau$, where the fault thickness L_τ is the finite distance between the two fault surfaces. Assuming these earthquakes also have compact shapes, we expect $D = 3$. Assuming also that the slip δ is defined by the smallest rupture dimension, Eq. (26) remains valid, so $\beta = 4$, and we expect a set of very small earthquakes for which, as per Eq. (25), $b = 1.125$. This is similar to results measured by Kwiatek et al. (2010), in which $1.1 < b < 1.21$ for post-blasting earthquakes with $-3.5 < m_w < -1.5$. A detailed analysis of these very small earthquakes is outside the scope of this paper, but warrants further study. This type of analysis may also be related to apparent deviations from traditional $b = 1$ GR scaling in catalogs with elevated rates of seismicity in advance of large earthquakes.

With respect to seismic hazard assessment, our findings are significant. On the one hand, this study produces no evidence of an upper limit to global earthquake magnitudes; large earthquakes occur with power-law probability for at least $m < 9$. On the other hand, earthquakes of $m > 7.6$ are substantially less common than traditional GR extrapolation, where universally $b = 1$, would suggest. According to traditional GR statistics, for example, the global recurrence interval Δt of the great $m = 9.5$ Chilean earthquake of 1960 is $\Delta t = 27$ years. That is to say, we should expect one $m >= 9.5$ earthquake to occur somewhere on the planet approximately every 27 years. According to Fig. 1, however, with $b_2 = 1.5$, the recurrence interval of an $m = 9.5$ earthquake is approximately $\Delta t = 217$ years.

We also show that the abrupt transition and power-law distribution in the domain $m > m_t$ indicate that rupture-fronts are smooth and that rupture shapes are compact. We show that the width L_w of a rupture acts as a characteristic size so that the rupture front propagates coherently, or equivalently from Eq. (34) $n_w \to 1$. This suggests that seismicity simulations such as AllCal (AC) (Ward, 1996, 2007) and Virtual California (VC) (Rundle et al., 2005) may require relatively sophisticated $d = 2$ models of fault surfaces and rupture propagation fronts. VC, a cellular automata model, for example may require high resolution in the depth direction of its fault system, and at the same time, its failure dynamics must be defined such that the rupture process transitions sharply from $D = 2$ to $D = 1$ when $L > W$. This transition depends on the shape of the rupture and will not occur for all rupture dynamics.

6. Conclusion

In conclusion, our findings are multifaceted. First, we show that earthquakes exhibit two distinct frequency–magnitude scaling domains. We measure $b = 1.009$ for $5.5 < m < 7.6$ and $b = 1.497$ for $7.6 < m < 9.0$, and we observe an abrupt transition between the two regimes. In addition to implications with respect to risk assessment, as discussed above, we show that this measurement corroborates theories of earthquake rupture based on constant stress-drop and geometrical constraints. Further, we show that the abrupt transition, in contrast to a gradual roll-over, between the two power-law regimes implies a smooth, fractal dimension $D \approx 1$, rupture front and implies that the rupture transitions abruptly from $D = 2$ to $D = 1$ when it encounters the upper and lower boundaries of the seismogenic zone. This suggests that finite element models of earthquake rupture can potentially improve speed performance by renormalizing their lattice to the size of the rupture.

The measured value of $b = 1.497$ for large earthquakes is consistent with the value predicted by Rundle (1989), $b = 1.5$, and also with Eq. (34), which implies that $b_2 \to 1.5$ from below. Note that Eq. (34) also implies $b_1 \to 1.0$ from above, which is consistent with our measured value $b = 1.009$. We further show that this transition does not require that $L_s \to \infty$, or equivalently from Eq. (34) $\alpha \to \infty$, so long as $n_w \to 1$ from above. That is to say, the transition from $b = 1.0$ to $b = 1.5$ occurs abruptly for $m \geq m_t$ ($L_s \geq W$) and does not require $m \gg m_t$ ($L_s >> W$). In combination, these conclusions have significant implications with respect to understanding and modeling regional seismicity and earthquake physics in general.

Acknowledgments

This research has been funded by the US Department of Energy grant DOE DE-FG02-04ER15568.

References

Aki, K., 1981. A probabilistic synthesis of precursory phenomena. In: Simpson, D.W., Richards, P.G. (Eds.), Earthquake Prediction, An International Review. : Maurice Ewing Series, 4. American Geophysical Union, pp. 566–574.

Aki, K., 1987. Magnitude–frequency relation for small earthquakes: A clue to the origin of f_{max} of large earthquakes. Journal of Geophysical Research 92, 1349–1355.

Bevington, P.R., Robinson, K.D., 1992. Data Reduction and Error Analysis for the Physical Sciences, 2nd edition. McGraw-Hill, Inc.

Burroughs, S.M., Tebbens, S.F., 2002. The upper-truncated power law applied to earthquake cumulative frequency magnitude distributions: evidence for a time-independent scaling parameter. Bulletin of the Seismological Society of America 92 (8), 2983–2993.

Carlson, J., Langer, J., 1989. Mechanical model of an earthquake fault. Physical Review A 40, 6470–6484.

Clark, T.L., Jenkins, M.A., Coen, J.L., Packham, D.R., 1996. A coupled atmosphere fire model: role of the convective Froude number and dynamic fingering at the fireline. International Journal of Wildland Fire 6, 177–190.

Drossel, B., Schwabl, F., 1992. Self-organized critical forest-fire model. Physical Review Letters 69 (11), 1629–1632 (Sep).

Frohlich, C., Davis, S.D., 1993. Teleseismic b values; or, much ado about 1.0. Journal of Geophysical Research 98 (B1), 631–644.

Gutenberg, B., Richter, C.F., 1954. Seismicity of the Earth and Associated Phenomenon, 2nd edition. Princeton Univ. Press.

Holliday, J.R., Yoder, M.R., 2012. A model for saturated power laws in geophysical systems. EPJ (in revision).

Jones, E., Oliphant, T., Peterson, P., et al., 2009. SciPy: open source scientific tools for Python. Software. . URL http://www.scipy.org.

Kanamori, H., Anderson, D.L., 1975. Theoretical basis of some empirical relations in seismology. Bulletin of the Seismological Society of America 65 (5), 1073–1095.

Kwiatek, G., Plenkers, K., Nakatani, N., Yake, Y., Dresen, G., 2010. Frequency–magnitude characteristics down to magnitude -4.4 for induced seismicity recorded at Mponeng gold mine, South Africa. Bulletin of the Seismological Society of America 100, 1165–1173.

Lay, T., Kanamori, H., 2011. Insights from the great 2011 Japan earthquake. Physics Today 64 (12), 33–39.

Pacheco, J.F., Scholz, C.H., Sykes, L.R., 1992. Changes in frequency–size relationship from small to large earthquakes. Nature 355, 71–73.
Romanowicz, B., Ruff, L., 2002. On moment-length scaling of large strike slip earthquakes and the strength of faults. Geophysical Research Letters 29 (12), 45-1–45-4.
Rundle, J., Rundle, P., Donnelan, A., Turcotte, D., Shcherbakov, R., Li, P., Malamud, B., Grant, L.B., Fox, G., Mcleod, D., Yakovlev, G., Parker, J., Klein, W., Tiampo, K., 2005. A simulation-based approach to forecasting the next great San Francisco earthquake. PNAS 102 (43), 15363–15367.
Rundle, J.B., 1989. Derivation of the complete Gutenberg–Richter magnitude–frequency relation using the principle of scale invariance. Journal of Geophysical Research 94 (B9), 12337–12342 (September).
Rundle, J.B., 1993. Magnitude–frequency relations for earthquakes using a statistical mechanical approach. Journal of Geophysical Research 98 (B12), 21943–21949.
Saleur, H., Sammis, C.G., Sornette, D., 1996b. Discrete scale invariance, complex fractal dimensions, and log-periodic fluctuations in seismicity. Journal of Geophysical Research 101 (B8), 17661–17677 (august).
Saleur, H., Sammis, C.G., Sornette, D., 1996a. Renormalization group theory of earthquakes. Nonlinear Processes in Geophysics 3, 102–109.
Shaw, B.E., 2009. Constant stress drop from small to great earthquakes in magnitude–area scaling. Bulletin of the Seismological Society of America 99 (2a), 871–875.
Shaw, B.E., Scholz, C.H., 2001. Slip-length scaling in large earthquakes: observations and theory and implications for earthquake physics. Geophysical Research Letters 28, 2995–2998.
Sornette, D., Knopoff, L., Kagan, Y., Vanneste, C., 1996. Rank-ordering statistics of extreme events: application to the distribution of large earthquakes. Journal of Geophysical Research 101 (B6), 13883–13893.
Stauffer, D., Aharony, A., 1994. Introduction to Percolation Theory, 2nd edition. Taylor and Francis, London.
Turcotte, D.L., Schubert, G., 2002. Geodynamics, 2nd edition. Cambridge University Press.
Ward, S.N., 1996. A synthetic seismicity model for southern California: cycles, probabilities, and hazard. Journal of Geophysical Research, Solid Earth 101 (B10), 22393–22418.
Ward, S.N., 2007. Methods for evaluating earthquake potential and likelihood in and around California. Seismological Research Letters 121–133.
Yoder, M.R., Turcotte, D.L., Rundle, J.B., 2011. A forest-fire model with natural fire resistance. Physical Review E: Statistical, Nonlinear, and Soft Matter Physics 83 (046118).